Electron. Mater. Lett., Vol. 13, No. 3 (2017), pp. 222-229
DOI: 10.1007/s13391-017-6038-4

Synthesis of $Sr_{(1-x-y)}Al_4O_7:Eu_x^{2+},Ln_y^{3+}$ (Ln = Dy, Y, Pr) Nanophosphors using Rapid Gel Combustion Process and their Down Conversion Characteristics

Devender Singh,[1,2,*] Vijeta Tanwar,[1] Anura Priyajith Samantilleke,[2] Bernabe Mari,[3] Shri Bhagwan,[1] Krishan Chander Singh,[1] Pratap Singh Kadyan,[1] and Ishwar Singh[1]

[1]Department of Chemistry, Maharshi Dayanand University, Rohtak 124001, India
[2]Centro de Fisica, Universidade of Minho, Braga 4710057, Portugal
[3]Departament de Física Aplicada, Universitat Politècnica de València, València 46022, Spain

(received date: 12 February 2016 / accepted date: 17 January 2017 / published date: 10 May 2017)

Eu^{2+} and Eu^{2+}+Ln^{3+} doped $SrAl_4O_7$ nanophosphors were synthesized by rapid gel combustion process. The morphology of prepared phosphors was examined with scanning and transmission electron microscopy. The phase identification and the crystal structures of nanophosphors were studied using X-ray powder diffraction techniques. Luminescence characteristics of the prepared nanophosphors were analyzed on account of excitation, emission and phosphorescence decay analysis. The emission spectra demonstrated the broad green emission attributed to $4f^65d^1 \rightarrow 4f^7$ transition of the Eu^{2+} ions. The effect of codoping of some trivalent lanthanide (Dy^{3+}, Pr^{3+} and Y^{3+}) ions were investigated for improving the emission intensity and phosphorescence decay time of the basic lattice of $SrAl_4O_7:Eu^{2+}$ phosphors. The synthesized materials had enhanced bright luminescent properties that could suitably be applied for display as well as photovoltaic applications.

Keywords: luminescence, $SrAl_4O_7:Eu^{2+}$, trivalent lanthanides, codopants, nanophosphor, XRD

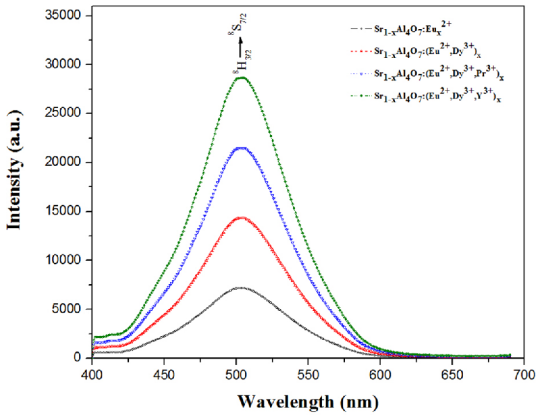

1. INTRODUCTION

During the last few years, lanthanide activated aluminate nanophosphors have been employed widely for many potential applications viz. in radiation dosimetry,[1] color display,[2] luminescent porcelain, luminous paints,[3] lamps[4] and flat panel devices.[5] Eu^{2+} activated alkaline earth aluminates materials find considerable attention due to bright luminescence in the visible region especially for the next generation of displays and lighting devices.[6,7] Li^+ is a well known coactivator which on incorporation enhances the luminescent efficiency of some phosphors lattices.[8-10] Earlier, ZnS:Cu,Co was used as a commercial persistent material which is now replaced by the $MAl_2O_4:Eu^{2+},Ln^{3+}$ (M = Ca and Sr).[11,12] Eu^{2+} ions play the role of luminescent center and Ln^{3+} ions act as coactivators in the lattice to increase the persistency in luminescence.[13,14] The persistent phosphorescence in the aluminate phosphor is due to the photoionization of the Eu^{2+} ion and a consequent migration of the electrons to the traps produced from the lattice defects of oxide ion vacancies or the supplementary Ln^{3+} ions.[15,16] It has been concluded in many findings that the Eu^{2+} ion act as a luminescent center for providing the blue (λ_{max} = 440)[17] and green (λ_{max} = 520) emission[18] in the spectral region for $CaAl_2O_4:Eu^{2+}$ and $SrAl_2O_4:Eu^{2+}$ correspondingly and the Ln^{3+} ions perform as a trap or to amend the trap properties of these materials.

The codoping of alkali or rare earth ions in the oxide lattices significantly enhance the emission intensity.[19-21] Also the intensity of emission and the long afterglow characteristics are drastically enhanced if codoped with

*Corresponding author: devjakhar@gmail.com

trivalent lanthanide ions, e.g., Dy^{3+} or Nd^{3+}.[22-24] Little work on the improvement of down conversion properties of $SrAl_4O_7$ phoshors had been reported yet, we developed a method for the instant preparation of nanosized particles to synthesize Eu^{2+} doped and trivalent lanthanide ions codoped $SrAl_4O_7$ nanophosphors using a rapid combustion techniques. The effect of coactivators on the optical characteristics of $SrAl_4O_7:Eu^{2+}$ nanophosphors have been studied. The down conversion properties and morphology of $SrAl_4O_7:Eu^{2+}$ codoped with Ln^{3+} (Dy^{3+},Pr^{3+},Y^{3+}) nanophosphors have been characterized fully.

2. EXPERIMENTAL PROCEDURE

2.1 Syntheses of nanophosphors

A series of nanophosphors $Sr_{(0.98)}Al_4O_7:Eu^{2+}{}_{(0.02)}$, $Sr_{(0.96)}Al_4O_7:Eu^{2+}{}_{(0.02)},Dy^{3+}{}_{(0.02)}$ and $Sr_{(0.96)}Al_4O_7:Eu^{2+}{}_{(0.02)},Dy^{3+}{}_{(0.01)},Ln^{3+}{}_{(0.01)}$ ($Ln^{3+} = Pr^{3+},Y^{3+}$) were synthesized by the rapid gel combustion procedure. The raw materials used in the experiment were of analytical grade. The preliminary materials $Sr(NO_3)_2$ (strontium nitrate), $Al(NO_3)_3{\cdot}9H_2O$ (aluminium nitrate nonahydrate), $Eu(NO_3)_3{\cdot}6H_2O$ (europium nitrate hexahydrate), Dy_2O_3 (dysprosium oxide), $Pr(NO_3)_3{\cdot}6H_2O$ (praseodymium nitrate hexahydrate), $Y(NO_3)_3{\cdot}6H_2O$ (yttrium nitrate hexahydrate) were used as the basic materials and NH_2CONH_2 (urea) was used as fuel. Dy_2O_3 was converted into nitrate form by adding the proper amount of dilute nitric acid till it dissolved and then evaporated. All the materials were mixed corresponding to their stoichiometric ratios. Boric acid (H_3BO_3) 12 mol percent against each mol percent europium present was used as a flux in order to optimize homogeneity and to get maximum brightness.[18] For these, stoichiometric compositions of the nitrates (called as oxidizers) and fuel (called as reducer) were calculated by using their total oxidizing as well as reducing valencies of the components.[25] The mixture was then dissolved in minimum water and stirred for ~10 minutes with warming to make a thick semi-solid paste. The paste was then put inside the preset muffle furnace at 600 °C. The reaction mixture melted, underwent dehydration and then finally decomposed with the evolution of numerous gases. The liberated gases swelled the mixture into large volume. The burning reaction accomplished within ~ 5 minutes. The final product thus obtained in the fluffy form was ground and used for the further characterizations. The chemical reaction underwent is shown as follows:

$$1\text{-}x\text{-}y[Sr(NO_3)_2] + 4Al(NO_3)_3.9H_2O + x(Eu(NO_3)_3.6H_2O + yLn(NO_3)_3.6H_2O + 6CO(NH_2)_2 + H_3BO_3(\text{flux}) \rightarrow Sr_{(1\text{-}x\text{-}y)}Al_4O_7:Eu_x^{2+},Ln_y^{3+} + 13N_2 + 6CO_2 + 48H_2O$$

2.2 Instrumentation

The morphology of the prepared materials was investigated with scanning electron microscopy (SEM) using Leo 435 VP scanning electron microscope and transmission electron microscopy (TEM) with a TECNAI 200 Kv (Fei, Electron Optics) transmission electron microscope. The crystalline phases of the powders were identified with X-ray diffraction analysis using Rigaku Ultima IV diffractometer with Cu-Kα radiation between wide ranges of Bragg angles ($10° \leq \theta \leq 70°$). Fourier Transform Infrared (FT-IR) spectra were taken using a Nicolet 5700 infrared spectrometer. X-ray photoelectron spectroscope PHI 5000 Versa Prob II was used for the characterization of the oxidation state of europium (either it exists in +2 or +3). Photoluminescence emission and excitation spectra were recorded on a Fluorimeter SPEX Fluorolog 1680 (USA) equipped with the SPEX 1934 D phosphorimeter using Xenon lamp as excitation source at room temperature.

3. RESULTS AND DISCUSSION

3.1 Morphological analysis

The microstructures of europium doped and rare earths codoped $SrAl_4O_7$ nanophosphors calcined at 600 °C were studied with scanning electron microscopy (SEM). The studies showed that the powder has irregular, foamy and agglomerate particles. The particles of prepared samples showed flake like morphology with non-uniform distribution as shown in Figs. 1(a-d). The foamy structure of the materials reflects the inherent nature of the combustion reaction of the metal nitrates occurred with fuel (urea) producing gases and huge amount of heat in the reaction. The surface of powder illustrates a large amount of voids and pores created due to the liberation of gases during combustion reaction (Figs. 1 (a-d)). Also, as the gases evolve, they leave a fluffy and crystalline fine powder.

Figures 2(a-d) display typical transmission electron microscope images of the synthesized strontium dialuminate crystals. TEM analysis has provided further more details of the nanostructures of the prepared nanophosphors. TEM micrographs signify that the phosphor materials contain extremely agglomerated nanocrystals. The average size is existing between 10-40 nm for these materials. The crystallite size of materials according to Scherrer's analysis is also found in good agreement with TEM observations, confirming the nanocrystallinity of the prepared materials.

3.2 X-ray diffraction patterns

The crystal phase structures of the synthesized phosphors were analyzed using X-ray diffraction patterns and are shown in Fig. 3. These XRD patterns match with standard (JCPDS) file number 70-1479 which can be indexed to monoclinic structure of $SrAl_4O_7$ lattice. These consequences also confirm that no change in the phase was seen co-doping with Ln^{3+} ions in the present method. Within sensitivity of XRD, no secondary phases were detected. The sharpness of

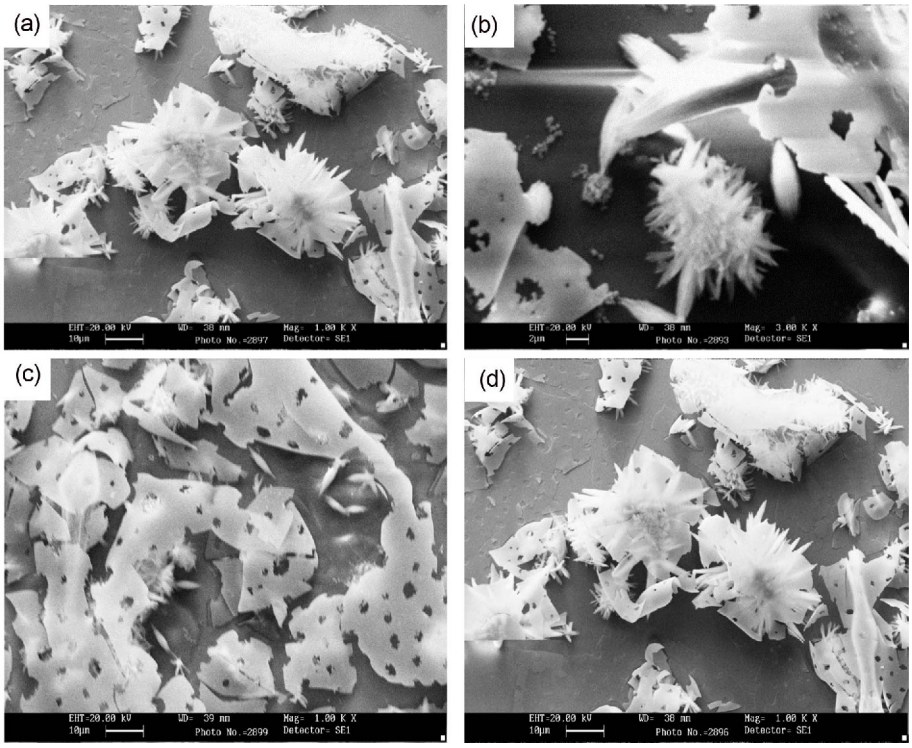

Fig. 1. SEM images of phosphors; (a) $SrAl_4O_7:Eu^{2+}$ (b) $SrAl_4O_7:Eu^{2+},Dy^{3+}$ (c) $SrAl_4O_7:Eu^{2+},Dy^{3+},Pr^{3+}$ (d) $SrAl_4O_7:Eu^{2+}$ Dy^{3+},Y^{3+}.

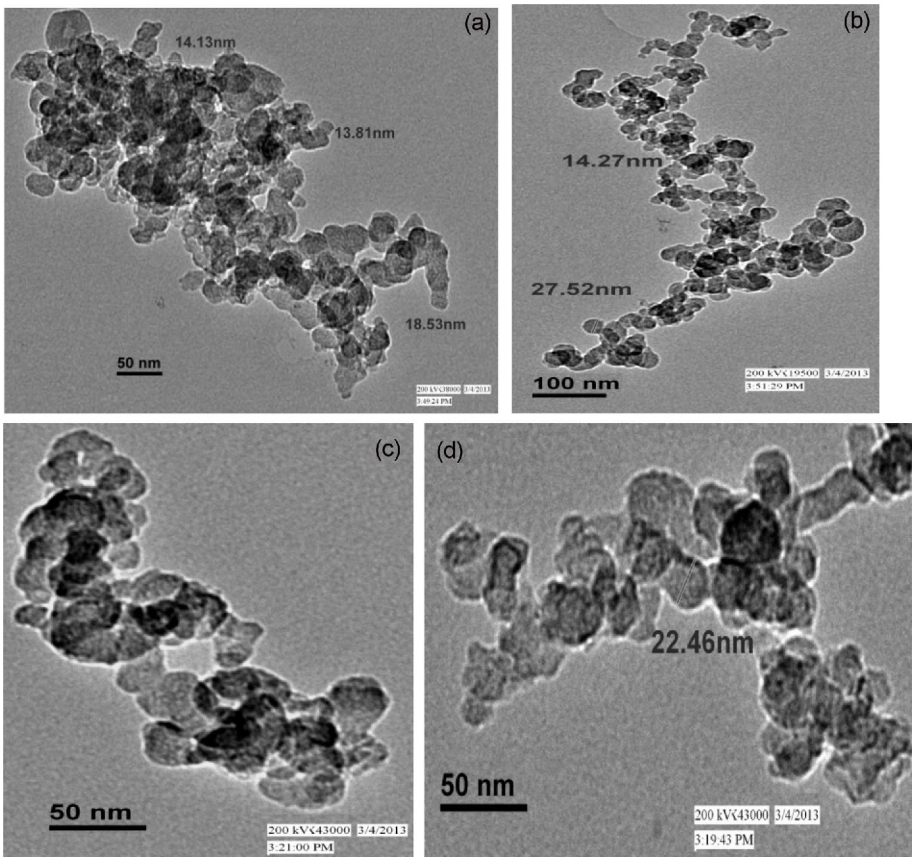

Fig. 2. TEM micrographs of nanophosphors; (a) $SrAl_4O_7:Eu^{2+}$ (b) $SrAl_4O_7$: Eu^{2+},Dy^{3+} (c) $SrAl_4O_7:Eu^{2+},Dy^{3+},Pr^{3+}$ (d) $SrAl_4O_7:Eu^{2+}$ Dy^{3+},Y^{3+}.

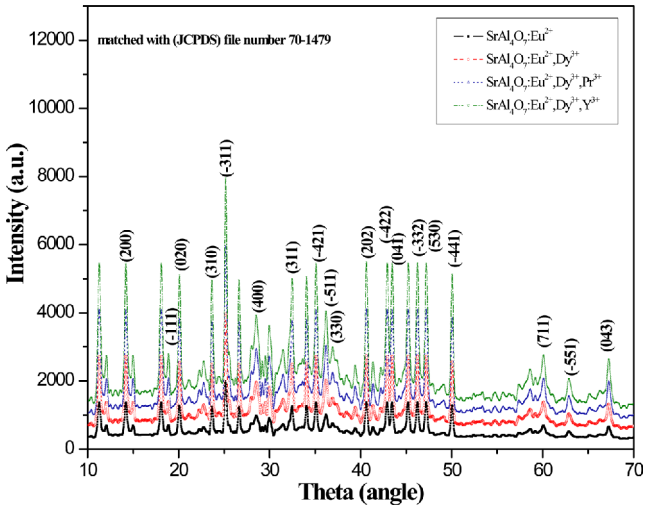

Fig. 3. X-ray diffraction patterns of prepared nanophosphors.

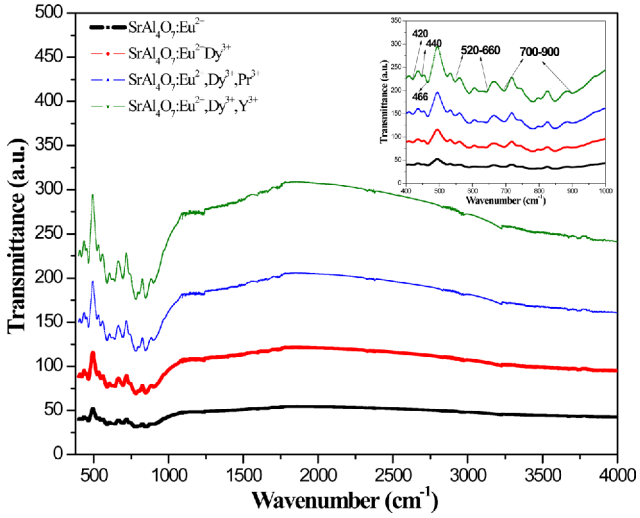

Fig. 4. FTIR spectra of the prepared materials.

Table 1. Calculated average size for the prepared nanophosphor crystallites.

Phosphor material	2θ value	Particle size
$SrAl_4O_7:Eu^{2+}$	25.20°	17.86 nm
$SrAl_4O_7:Eu^{2+},Dy^{3+}$	25.22°	23.82 nm
$SrAl_4O_7:Eu^{2+},Dy^{3+},Pr^{3+}$	24·84°	36.08 nm
$SrAl_4O_7:Eu^{2+},Dy^{3+},Y^{3+}$	25.00°	30.12 nm

diffraction peaks designates the crystallinity of the nanomaterials. These patterns belong to C2/*c* space group consisting of AlO_4 tetrahedra and AlO_6 octahedra with crystal structure of $SrAl_4O_7$. Interlinked layers of AlO_4 tetrahedra expand in the xy-plane. The Sr ions and the AlO_6 octahedra act as connecting bridges between the layers. Each AlO_4 tetrahedra is linked to four neighbors through a shared oxygen atom. It is considered that the Eu ions (rEu^{2+} = 1.09 A°) substituted the Sr ions (rSr^{2+} = 1.12 A°) due to their close matched ionic radii. The activators have no other effects on incorporating to host lattices except the enhancement in intensities. The crystallite sizes calculated from the XRD patterns of prepared materials using Scherrer formula are shown in Table 1.

3.3 FTIR analysis

Figure 4 shows the FTIR spectra of the samples of Eu^{2+} doped and Ln^{3+} (Dy^{3+}, Pr^{3+} and Y^{3+}) codoped phosphor materials prepared. The spectra of the samples are taken in the 4000-400 cm^{-1} region. A doublet at 440 cm^{-1} and 420 cm^{-1} appeared owing to the symmetric bending of O-Al-O. Two quartets, one for antisymmetric stretching (700-900 cm^{-1} region) and another for antisymmetric bending (520-660 cm^{-1}) are obtained for O-Al-O which confirms the existence of AlO_4^- tetrahedral unit. The peaks in the region of 700-800 cm^{-1} are accredited to the Sr-O bond vibrations. In aluminate phosphors, the lattice structure is constructed by AlO_4^- tetrahedral and the interstitial spaces are filled with Sr^{2+} ions. Dopants (Ln^{3+}-Dy^{3+}, Pr^{3+} and Y^{3+}) ions are expected to replace Sr^{2+} sites available in the host lattice. Some studies indicated that the crystal undergo lattice stress because of doping when used in the higher concentration (more than 10 mole %).[26-31] In the present work we used 12 mol percent of the boric acid and less than 5% of dopant as well as codopants to obtain desirable properties of the phosphor materials. A minor shift in the peaks is explained[28-31] due to the difference in mass number of dopant and lattice ions. The difference in mass of ions leads to a change in the molecular geometry and mechanical vibrations, which results in a shift in bands.[29-31] Special characteristics peaks have been not observed in the FTIR spectra of these prepared materials. Incorporation of higher concentration of dopants (more than 10 mole %) would have produced some characteristics peaks in their respective spectra (FTIR).

3.4 X-ray photoelectron (XPS) analysis

The sample by XPS studies were characterized for diagnosing the oxidation states of the europium. Peaks for all the elements of $SrAl_4O_7:Eu^{2+}$ phosphors (Fig. 5) are in accordance with standard consequent values of peak positions. The peaks accredited to Eu 3d, Sr 3d, O 1s and Al 2p core levels are observed in XPS spectra. The single peak obtained at 531.8 eV is specified to the O (1s).[32] The Al (2s) and Al (2p) are located virtually at 133.3 eV and 89.1 eV, respectively. The XPS spectra of $SrAl_4O_7:Eu^{2+}$ phosphor recognized the occurrence of Eu^{2+} having one characteristics peak at 1126.4 eV and another at ~1153.4 eV, which are ascribed to Eu^{2+} $3d_{5/2}$ and $3d_{3/2}$ respectively. $3d_{5/2}$ and $3d_{3/2}$ peaks at 1134 and 1165 eV respectively are absent in the

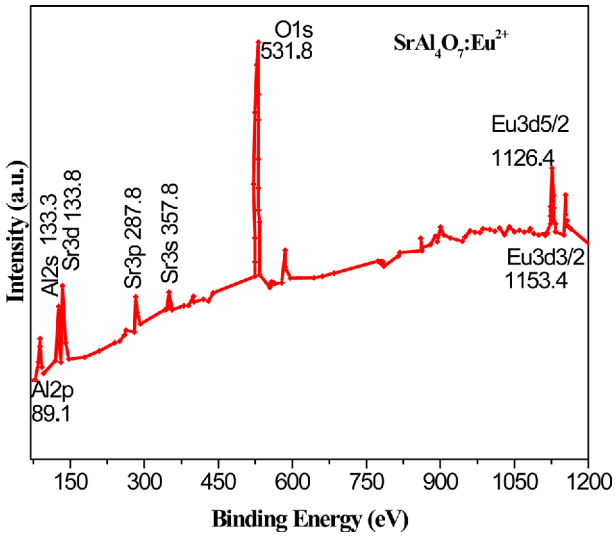

Fig. 5. X-ray photoelectron analysis of $SrAl_4O_7:Eu^{2+}$.

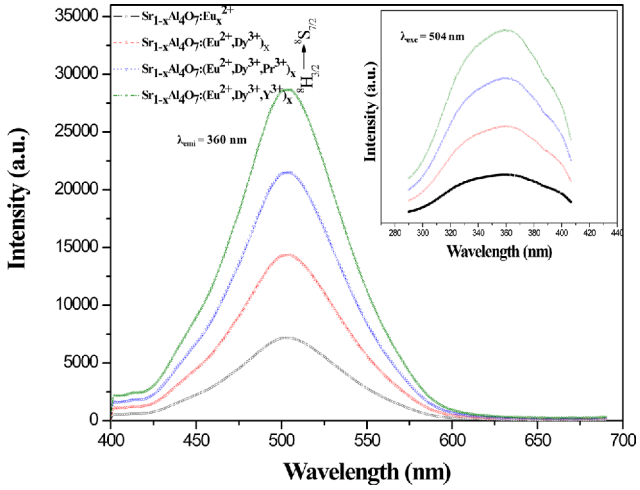

Fig. 6. Emission spectra of synthesized phosphors and inset shows the excitation spectra.

spectra which proves the absence of Eu^{3+}.[33-35] Hence the oxidation state of doped europium exists in divalent state in the prepared phosphor. Sr 3s, Sr 3p and Sr 3d are positioned at 357.8, 287.8 and 133.8 eV, correspondingly.

3.5 Photoluminescence properties of parent host $SrAl_4O_7:Eu^{2+}$

Upon excitation in near UV region (360 nm) a broad band emission spectra is obtained at 504 nm. The emission in green region designate that the doped Eu exists in +2 states, not in +3 states as there is no special emission of red color (~612 nm of $^5D_0 \rightarrow {}^7F_2$ transition) of Eu(III) in the photoluminescence spectra. On addition of boric acid in sample synthesis, a tetrahedral borate [BO_4] unit increases while the tetrahedral aluminate [AlO_4] unit gradually decreases.[36] As the radius of B^{3+} is smaller in comparison to Al^{3+} so the B-O bond (Bond length of B-O 1.25 A° having bond dissociation energy of 806 KJ/mol) is stronger than that of Al-O bond (bond length of Al-O 1.60 A° having bond dissociation energy of 512 KJ/mol).[2,26,27,37-40] Thus, as compared to [AlO_4] unit, [BO_4] unit provide much more compactness to the lattice that resulted in the shrinkage of the host lattice of these materials.[2,26,38-40] The three-dimensional rigid networks having the more compact borate units protect Eu^{2+} from aerial oxidation more effectively in comparison to aluminate units. Due to that, enhanced luminescence is observed in emission spectra from Eu^{2+} ions.[41] For the maintenance of the electroneutrality of the compound, three Sr^{2+} ions could be replaced by only two Eu^{3+} ions. A negative Sr^{2+} vacancy is created which could work as an electron donor. Consequently, the anomalous reduction is accredited to an electron transfer from this thermal stimulated defect to Eu^{3+}. It is supposed that as more electrons on strontium vacancies are produced, the more reduction of Eu^{3+} ions would occur in compounds. This reduction mechanism is more conferred in codoping experimental results.[42] The anion BO_4^{5-} tetrahedra are supposed to provide an electron for the reduction of trivalent europium into divalent europium.[43]

Figure 6 is showing the emission and excitation (inset) spectra of $SrAl_4O_7:Eu^{2+}$. The excitation spectra show a broad band from 290-410 nm corresponding to the d orbital splitting of Eu(II). The excitation spectrum is attributed due to $4f^7 \rightarrow 4f^65d^1$ transition of Eu^{2+}. The emission spectrum has a broad peak centered at 504 nm accredited due to $4f^65d^1 \rightarrow 4f^7$ transition of Eu^{2+} ions which is a permissible electrostatic dipole transition. The wide emission band is because of the involvement of 5d orbital in crystal field splitting of Eu^{2+}. However, in absence of coactivator (Trivalent ions i.e. Dy^{3+}, Pr^{3+}, Y^{3+}) no phosphorescence property is observed in the parent host.

3.5.1 Photoluminescence and phosphorescence properties of $SrAl_4O_7:Eu^{2+},Ln^{3+}$ with trivalent codopants (Dy^{3+}, Pr^{3+}, Y^{3+})

The emission and excitation (inset) spectra of Eu^{2+} doped and codoped with some Ln^{3+} ions $SrAl_4O_7$ nanophosphors are shown in Fig. 6. These phosphors demonstrated strong absorption in the UV region and emitted a green light under excitation of UV light. When Dy^{3+}, Pr^{3+} and Y^{3+} are used as codopants in the lattices, the form and position of the spectral peaks remained at same places, however intensities get enhanced. The broadening of emission peaks for the codoped samples is ascribed to the variations of crystal field strength around Eu^{2+} ions, when Dy^{3+}, Pr^{3+} and Y^{3+} ions also incorporated. The outer 5d orbital of the Eu^{2+} can be affected strongly by the crystal field. Consequently the $4f^65d^1$ energy value can be extended into a continuous broad emission

band. This proves that Eu^{2+} is the only luminescent centre in the phosphors whereas Dy^{3+}, Pr^{3+} and Y^{3+} facilitate enhancement of luminescence. The special codopants emission peaks are not present in the spectra; therefore codopants may possibly be recognized having the role of energy transportation (electron traps). The emission intensity of phosphors increased with the addition of codopants and the maximum intensity approached when both Dy^{3+}+Y^{3+} are used as codopants possibly developing the traps and increasing their trap depth which help in the energy transportation.[26,27,44,45] In present condition, the energy transfer takes place from one dopant to another till the utilization of energy. Codopants ions Dy^{3+}, Pr^{3+} and Y^{3+} induced the development of energy trap levels which prolonged the phosphorescence. There are two sites existing for the codopants (Dy^{3+}, Pr^{3+} and Y^{3+}) in the present lattice of $SrAl_4O_7$ either Sr^{2+} or Al^{3+} sites. Ionic radius of Sr^{2+} (0.112 nm) are analogous to the ionic radius of Eu^{2+}, Dy^{3+}, Pr^{3+} and Y^{3+}. With the addition of boric acid, deep penetration of rare earth ions into the lattice takes place because of low melting point of B_2O_3. This provides a liquid medium which helped the codopants to diffuse in deep into the lattice and also facilitate the existence of Eu^{2+} ions as active centers for the present host aluminate lattice.[46] Therefore, homogenous and deep distribution of the dopant and codopants takes place in the entire matrix. This improves the dopant ions concentration in the host matrixes, which enhanced the luminescence characteristics and are useful for the various photovoltaic applications as well.

3.5.2 Mechanism of afterglow

Eu^{2+}, Ln^{3+} exhibit comparatively elevated luminescence intensity for a longer period. This can be explained in two ways: first one is that the coactivated Ln^{3+} ions efficiently transfer the absorbed energy to the Eu^{2+} emitter. Second way is the depth of traps formed by the coactivated Ln^{3+} ions is more appropriate. In these figures(6, 8), the PL intensity is found to be increase with the addition of codopants. Long duration phosphorescence is supposed due to the thermally released electrons from the traps, with the divalent europium as emitting centers. Consequently, the long persistent luminescence of the $SrAl_4O_7$:Eu^{2+}, phosphors is affected due to the depth and density of traps, which developed because of Ln^{3+} codopants. The mechanism of afterglow is attributable due to the trapped, transported and detrapped procedure of the electrons as suggested by Emen *et al.*[27,47] and are also observed in our studies as shown in Fig. 7. Ln^{3+} ion helps in the development of the traps for the electrons which exist in the excited and ground state of Eu(II) ions. When the material is under the UV excitation the election start escaping from Eu^{2+} to the conduction band of $SrAl_4O_7$ and Eu^{2+} would be converted to Eu^{3+}. The escaped electrons are trapped with Dy^{3+} to produce Dy^{2+}. As soon as the UV light source

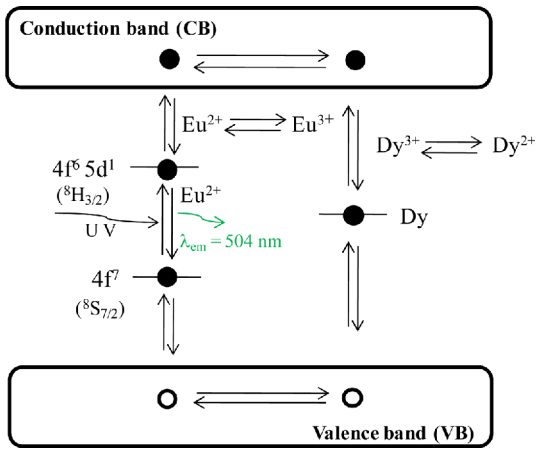

Fig. 7. Probable mechanism of afterglow of nanophosphor.

Table 2. Showing the color coordinates of synthesized nanophosphors.

Phosphor compounds	Color coordinates
$SrAl_4O_7$:Eu^{2+}	x-0.16792, y-0.40491
$SrAl_4O_7$: Eu^{2+},Dy^{3+}	x-0.17465, y-0.4429
$SrAl_4O_7$:Eu^{2+},Dy^{3+},Pr^{3+}	x-0.16157, y-0.5138
$SrAl_4O_7$:Eu^{2+},Dy^{3+},Y^{3+}	x-0.16287, y-0.5438

removed, a slow release of the electron followed by re-trapping on Eu and the creation of the emission due to $4f^6 5d^1 \rightarrow 4f^7$ which lead to the persistent afterglow of these nanomaterials. It is indicated that the Ln^{3+} ions facilitate the traps developed in the phosphors.[26,27,39] The emissive colors were established by use of the Commission Internationale de Eclairage (CIE) coordinate diagram. The calculated color coordinates are shown in Table 2 consequent to green color in the visible region on the color triangle.

The phosphorescence lifetime decay curves of $SrAl_4O_7$:Eu^{2+}, along with trivalent lanthanide ions (Dy^{3+}, Pr^{3+} and Y^{3+}) have been evaluated by curve fitting and these are fitted successfully based on the exponential equation. The decay outline of Ln^{3+} and Eu^{2+} emission of $SrAl_4O_7$ was measured using an excitation source of wavelength 360 nm and shown in Fig. 8. Variation is shown in the decay time with the various coactivators. Decay time of singly activated sample is exponential whereas on addition of coactivators the decay curves are found nonexponential. The life times of the Ln^{3+} and Eu^{2+} emission are deliberated with the equation as:

$$I = A_0 + A_1\exp(-t/\tau_1) + A_2\exp(-t/\tau_2) \quad (1)$$

where I is phosphorescence intensity; A_0, A_1 and A_2 are the constants, t is time, and τ_1, τ_2 are the exponential components of luminescent lifetime, respectively.

The liquid phase sintering is aided by the flux to help the particle growth of the strontium aluminates and increase the

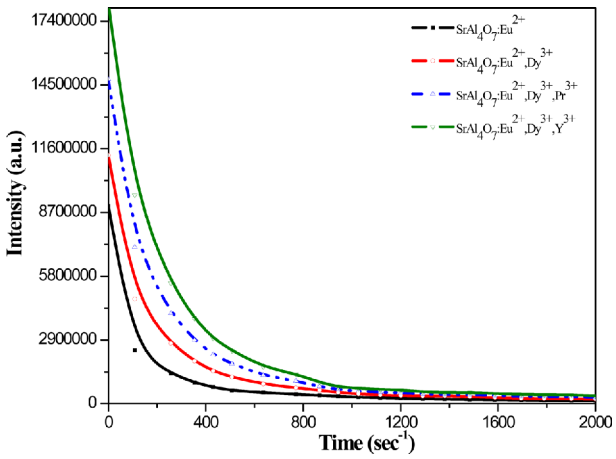

Fig. 8. Decay spectra of the synthesized nanophosphors.

development of trap centers in these phosphor materials. The increased amount of Dy^{3+} ions in the host increased the trapping capacity that enhances the phosphorescence intensity and its depth or the release rate of trapped electrons control the afterglow duration.[48,49] Hence, the dissolved B^{3+} ions reinstate Al^{3+} ions in tetrahedral sites. This substitution consequences in the reduction of lattice and enhances the trapping power of Dy^{3+} that enhances the afterglow intensity. The decay curve exhibited growth in starting and after that decayed, which could be fitted into a bi-exponential. The phosphorescence perceived in prepared materials could be ascribed to energy exchange occurred among traps and emission states of Eu, Dy, Pr and Y ions. The decay phenomenon of luminescence is very complex accredited to the numbers of traps and their depth. The Dy^{3+} integration created deep traps in the energy band gap of the host matrix.[50] The sensitizer ions Pr^{3+} and Y^{3+} also acted as traps and the trap levels positioned close to the valence band. The codopants traps captured some of the free electrons moving in the valence band due to the excitation of light source. On switching off the excitation source, a few electrons detained by the codopants traps are gradually released thermally and then relaxed to the excited state of Eu^{2+}, finally returning back to the ground state of Eu(II) with the emission of light (504 nm). Such studies of long persistence development owing to the trapped- transported-detrapped process is also very useful for the photovoltaic application.[27,45,47]

4. CONCLUSIONS

The nanophosphors were prepared successfully using the rapid gel combustion procedure. Phosphorescence was observed in all the phosphors developed with trivalent lanthanide ions incorporated as codopants. The phosphors were characterized for the effect of coactivator ($Ln^{3+} = Dy^{3+}$, Pr^{3+}, Y^{3+} ions) on the optical characteristics of $SrAl_4O_7:Eu^{2+}$ nanomaterials. The enhanced down conversion properties of the $SrAl_4O_7:Eu^{2+}$ nanophosphors were found to be improved with the incorporation of Ln^{3+} codopants in the present host matrix. Codoping of Dy^{3+}, Pr^{3+} and Y^{3+} ions improved the phosphorescence decay lifetime of the Eu^{2+} ions. The Ln^{3+} codoped $SrAl_4O_7:Eu^{2+}$ phosphor revealed excellent phosphorescence characteristics, demonstrating that a deeper trap centers were produced in the present phosphor lattice. Maximum down conversion properties and maximum phosphorescence behaviour were found in case of $SrAl_4O_7:Eu^{2+}$, Dy^{3+}, Y^{3+} nanophosphor. These phosphorescent materials having excellent chemical stability could be applied for lightening as well as photovoltaic applications.

ACKNOWLEDGEMENTS

The authors thankfully recognize the financial support from the University Grant Commission (UGC), New Delhi [MRP-40-73/2011(SR)] and the European Commission through Nano CIS project (FP7-PEOPLE-2010-IRSES ref. 269279).

REFERENCES

1. B. Zhang, C. Zhao, and D. Chen, *J. Bio. Chem. Lumin.* **25**, 25 (2010).
2. A. Nag and T. R. N. Kutty, *J. Alloys Compd*. **354**, 221 (2003).
3. S. H. Choi, N. H. Kim, Y. H. Yun, and S. C. Choi, *J. Ceram. Process. Res.* **7**, 62 (2006).
4. B. M. Smets, *Mater. Chem. Phys*. **16**, 283 (1987).
5. C. R. Ronda, *J. Lumin*. **72-74**, 49 (1997).
6. V. Chernov, T. M. Piters, R. Melendrez, W. M. Yen, E. Cruz-Zaragoza, and M. Barboza-Flores, *Radiat. Meas*. **42**, 668 (2007).
7. S. Chawla, N. Kumar, and H. Chander, *J. Lumin*. **129**, 114 (2009).
8. T. Hatayama, S. Fukumoto, and S. Ibuki, *Jpn. J. Appl. Phys.* **31**, 3383 (1992).
9. O. A. Lopez, J. McKittrick, and L. E. Shea, *J. Lumin*. **71**, 1 (1997).
10. H. K. Yang, J. W. Chung, B. K. Moon, B. C. Choi, and J. H. Jeong, *J. Korean Phys. Soc*. **52**, 116 (2008).
11. T. Katsumata, T. Nabae, K. Sasajima, S. Komuro, and T. Morikawa, *J. Am. Ceram. Soc.* **81**, 413 (1998).
12. R. Sakai, T. Katsumata, S. Komuro, and T. Morikawa, *J. Lumin*. **85**, 149 (1999).
13. V. Singh, J. J. Zhu, M. K. Bhide, and V. Natarajan, *Opt. Mater.* **30**, 446 (2007).
14. X. M. Teng, W. D. Zhuang, and H. Q. He, *Rare Metals* **27**, 335 (2008).
15. C. Zhao and D. Chen, *Mater. Lett*. **61**, 3673 (2007).
16. Y. Lin, Z. Tang, Z. Zhang, and C. Nan, *J. Eur. Ceram. Soc.*

23, 175 (2003).
17. D. Singh, V. Tanwar, A. P. Simantilleke, B. Mari, P. S. Kadyan, and I. Singh, *Adv. Mater. Lett.* **7**, 47 (2016).
18. D. Singh, V. Tanwar, A. P. Simantilleke, B. Mari, S. Bhagwan, P. S. Kadyan, and I. Singh, *J. Electron. Mater.* **45**, 2718 (2016).
19. J. C. Park, H. K. Moon, D. K. Kim, S. H. Byeon, B. C. Kim, and K. S. Suh, *Appl. Phys. Lett*. **77**, 2162 (2000).
20. M. Gu, L. Xiao, X. Liu, R. Zhang, B. Liu, and X. Xu, *J. Alloys Compd*. **426**, 390 (2006).
21. L. Wanga and Y. Wang, *J. Lumin*. **122**, 921 (2007).
22. C. Cai, P. Wen, L. Hao, and X. Xu, *Mater. Res. Bull*. **55**, 156 (2014).
23. S. Unithrattil, K. H. Lee, and W. B. Im, *J. Am. Ceram. Soc*. **97**, 874 (2014).
24. H. Yamamoto and T. Matsuzawa, *J. Lumin*. **72-74**, 287 (1997).
25. S. Ekambaram and K. C. Patil, *J. Alloys Compd.* **248**, 7 (1997).
26. J. Chen, F. Gu, and C. Li, *Cry. Growth Des.* **8**, 3175 (2008).
27. G. I. Akmehmet, S. Sturm, L. Bocher, M. Kociak, B. Ambrozic, and C. W. O. Yang, *J. Am. Ceram. Soc.* **99**, 2175 (2016).
28. K. D. Giras, *J. Nano-Electron. Phys.* **5**, 03013 (2013).
29. S. Suri, K. K. Bamzai, and V. Singh, *J. Therm. Anal. Calorim.* **105**, 229 (2011).
30. S. J. Joshi, B. B. Parekh, K. D. Vohra, and M. J. Joshi, *Bull. Mater. Sci.* **29**, 307 (2006).
31. I. Quasim, A. Firdous, N. Sahni, S. K. Khosa, and P. N. Kotru, *Cryst. Res. Technol.* **44**, 539 (2009).
32. S. M. Lee, T. Ito, and H. Murakami, *Proc. Annual Autumn Conference on the Korea Institute of Electrical and Electronic Material Engineers*, p. 705, Seoul, Republic of Korea (2003).
33. W. B. Im, J. H. Kang, D. C. Lee, S. Lee, D. Y. Jeon, Y. C. Kang, and K. Y. Jung, *Solid State Commun*. **133**, 197 (2005).
34. J. Zhang, M. Yang, H. Jin, X. Wang, X. Zhao, X. Liu, and L. Peng, *Mater. Res. Bull.* **47**, 247 (2012).
35. P. Maślankiewicz, J. Szade, A. Winiarski, and Ph. Daniel, *Cryst. Res. Technol*. **40**, 410 (2005).
36. D. Singh, V. Tanwar, A. P. Simantilleke, B. Mari, P. S. Kadyan, and I. Singh, *J. Mater. Sci. Mater. Electron.* **27**, 2260 (2016).
37. T. L. Cottrell, *The Strengths of Chemical Bonds*, Butterworth, London, UK (1958).
38. C. Zhu, Y. Yang, X. Liang, S. Yuan, and G. Chen, *J. Am. Ceram. Soc.* **90**, 2984 (2007).
39. F. Clabau, X. Rocquefelte, S. Jobic, P. Deniard, M. H. Whangbo, A. Garcia, and T. Le Mercier, *Chem. Mater.* **7**, 3904 (2005).
40. Q. Zeng, Z. Pei, and Q. Su, *J. Alloys Compd*. **275**, 238 (1998).
41. H. Zeng, Y. Yang, Z. Lin, X. Liang, S. Yuan, G. Chen, and L. Sun, *J. Non-Cryst. Solids* **357**, 2328 (2011).
42. B. Liu, Y. Wang, J. Zhou, F. Zhang, and Z. Wang, *J. Appl. Phys*. **106**, 053102-1 (2009).
43. I. C. Chen and T. M. Chen, *J. Mater. Res*. **16**, 644 (2001).
44. A. Jain, A. Kumar, S. J. Dhoble, and D. R. Peshwe, *Renew. Sustainable Energy Rev.* **65**, 135 (2016).
45. Y. Li, M. Gecevicius, and J. Qiu, *Chem. Soc. Rev.* **45**, 2090 (2016).
46. Y. L. Chang, H. I. Hsiang, and M. T. Liang, *J. Alloys Compd*. **461**, 598 (2008).
47. F. M Emen, N. Külcü, and A. N. Yazici, *Eur. J. Chem.* **1**, 28 (2010).
48. J. S. Bae, J. H. Jeong, S. S. Yi, and J. C. Park, *Appl. Phys. Lett*. **82**, 3629 (2003).
49. P. Dorenbos, *Phys. Status Solidi* **242**, R7 (2005).
50. J. Zhang, J. Lin, J. Wu, S. Zhang, P. Zhou, X. Chen, and R. Xu, *J. Mater. Sci. Mater. Electron.* **27**, 1350 (2016).